NiCo$_2$O$_4$/Ag as catalyst for bi-functional oxygen electrode

D. Nicheva[1,2], B. Abrashev[1], I. Piroeva[3], V. Boev[1], T. Petkova[1], P. Petkov[2], K. Petrov[1]

[1]*Institute of Electrochemistry and Energy Systems Acad.E.Budevski, Bulgarian Academy of Sciences, Bl.10 Acad. G. Bonchev Str., 1113 Sofia, Bulgaria*
[2]*University of Chemical Technology and Metallurgy, 8, St. Kliment Okhridski Blvd., 1756 Sofia, Bulgaria*
[3]*Institute of Physical Chemistry, Bulgarian Academy of Sciences, Bl. 11 Acad. G. Bonchev Str.,1113 Sofia, Bulgaria*

NiCo$_2$O$_4$ has been synthesized using precipitation reaction. The obtained material studied by X-ray diffraction and scanning electron microscopy exhibits spinel structure. The electrochemical performance of the electrodes prepared from NiCo$_2$O$_4$ and NiCo$_2$O$_4$/Ag has been investigated by cyclic voltammetry, steady-state measurements and charge/discharge tests. The results demonstrate good electrochemical activity of the catalysts both in oxygen evolution and oxygen reduction reaction - the NiCo$_2$O$_4$/Ag electrode is stable more than 400 charge/discharge cycles.

Keywords: nickel-cobaltite, precipitation reaction, bi-functional oxygen electrode

INTRODUCTION

Innovative rechargeable batteries that can effectively store renewable energy are subject of increasing development. Among various metal/air batteries, the zinc/air battery is a system proven to have the required capacity for numerous applications. The rechargeable Zn-air batteries have focused the efforts of the researchers not only due to considerably high energy density but also due to cost efficiency. The theoretical calculated specific energy density of Zn-air batteries is 1084 Wh.kg^{-1}. [1-3].

The main challenge in the Zn/Air batteries progress is associated with the problems of zinc anode: dissolution into the alkaline solution [4], corrosion and the dendrite formation [5]. In rechargeable metal-air batteries, the oxygen evolution reaction (OER) and oxygen reduction reaction (ORR) both occur on the same electrode (usually the positive electrode) during the charge and discharge processes, respectively. The barriers for the bi-functional oxygen electrodes (BOE) are connected with: (i) the irreversibility of the oxidation reaction; (ii) corrosion during OER and (iii) the need of catalysts for both reactions – OER and ORR.

The efforts to develop oxygen electrode catalysts that operate both in cathodic and anodic modes are met by the irreversibility of both oxygen and evolution reactions in aqueous media at moderate temperatures (<150 °C) and composition limitations. The material used for a bi-functional oxygen electrode should be good catalysts for both the oxidation and reduction reactions of oxygen and should be chemically stable over the wide range of potentials experienced during charge and discharge. Several attempts to construct bi-functional oxygen electrode (BOE) using metallic catalysts in a multi-layered design have been made but no commercially available material have appeared yet. The need of more efficient and corrosion resistant catalyst materials still exists and various metal oxides have been investigated as bi-functional catalysts for oxygen electrodes last years [6-11].

It is important to develop efficient bifunctional catalysts for both ORR during discharge and OER during charge. For ORR in alkaline electrolytes, Ag is known to be very active. Its activity can be increased by modification with other metals as NiCo$_2$O$_4$. The spinel nickel cobaltite (NiCo$_2$O$_4$) catalyst has focused much attention due to their cost-efficiency and availability but also due to the better electrical conductivity and electrochemical activity in comparison to other binary transition metal oxides [12, 13].

This paper describes our results in preparation of a non-precious metal hybrid as bi-functional catalysts for ORR and OER by mixing a catalyst which has superior activity for ORR (Ag) with one which is highly active and stable for OER (NiCo$_2$O$_4$) as.
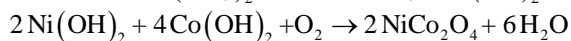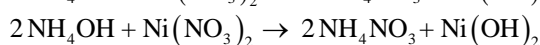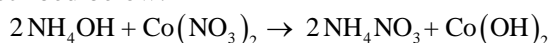
EXPERIMENTAL

1. Synthesis

NiCo$_2$O$_4$ was synthesised by precipitation technique: solutions of Co(NO$_3$)$_2$.6H$_2$O and Ni(NO$_3$)$_2$.6H$_2$O were mixed with NH$_4$OH in appropriate amounts at room temperature. The resultant precipitate, after filtration, was washed

---

* To whom all correspondence should be sent.
E-mail: d.vladimirova@iees.bas.bg

with distilled water and dried for 2 hours. The obtained product was slowly heated with a rate of 1°C/min in air up to 350 °C for 4 hours. The reactions occurring during the synthesis are described below:

$$2\,NH_4OH + Co(NO_3)_2 \rightarrow 2\,NH_4NO_3 + Co(OH)_2$$

$$2\,NH_4OH + Ni(NO_3)_2 \rightarrow 2\,NH_4NO_3 + Ni(OH)_2$$

$$2\,Ni(OH)_2 + 4\,Co(OH)_2 + O_2 \rightarrow 2\,NiCo_2O_4 + 6\,H_2O$$

Silver powder was prepared by reduction method using the procedure reported by Carey [14] from iron sulfate, sodium citrate and sodium base mixed with silver nitrate solution under vigorous stirring. The obtained precipitate was filtered, washed with ammonium nitrate and ethyl alcohol and dried in the open air.

2. Characterization

XRD patterns were recorded by X-ray diffractometer (Philips APD-15) at ambient temperature with a constant step of $0.02\ s^{-1}$ in the range $2\theta = 20°$- $80°$ at wavelength $\lambda = 1.54178$ Å using a CuKα tube. The Rietveld refinement of the experimental data was performed using the MAUD program.

The microstructure was studied using JSM 6390 scanning electron microscope (Japan) equipped with ultrahigh resolution scanning system (ASID-3D) in regimes of secondary electron image (SEI) and back scattered electrons (BSE) image. The measurements were performed with an accelerating voltage of 20 kV, power of ~65 mA and pressure - 10^{-4} Pa.

3. Electrochemical tests

The electrochemical behaviors of the electrodes were examined by cyclic voltammetry (CV), steady-state measurements and charge/discharge tests. Cyclic voltammetry and steady state curves were recorded using Solartron Schumberger 1820 potentiostat and Tacussel (Bi-PAD), supplied by a commercial software. Inert gas (N₂) was purged through the gas-permeable layer during the cycling. The study was carried out in three-electrode electrochemical setup consisting of working electrode (WE), platinum plate counter electrode (CE), and hydrogen electrode as a reference electrode (RE) ("Gascatel"). All tests were carried out at room temperature in electrolyte of 6M KOH aqueous solution.

CV tests were performed in the voltage range of -0.5 +1.5 V (RHE) at scan rate of $50\,mVs^{-1}$.

Charge/discharge tests were performed using three-electrode cell designed by us [15], eight channel Galvanostate 54 (PMC) working in the potential range -1,0 V + 2 V and charge/discharge

current density of $\pm10\,mA/cm^{-2}$. The experiment was completed in 6M KOH solution with duration: charge time - 45 min, discharge time -30 min.

4. Electrode preparation

Two WE were prepared: electrode I with NiCo₂O₄ as catalytic material and electrode II – with catalytic material mixture of NiCo₂O₄/Ag.

Working electrode (WE) with geometric surface area of 10cm² was fabricated by pressing of 40 mg/cm² active catalytic layer on the current collector (nickel mesh). The composition of the active layer was: 70 wt.% Ag , 20 wt. % NiCo₂O₄ or NiCo₂O₄/Ag mixed with 10 wt. % PTFE (Teflon emulsion, Sigma Aldrich)), 50 mg/cm² conductive agent and binder (teflonized Vulcan XC72 carbon black (Cabot Corporation).

RESULTS AND DISCUSSION

The X-ray analysis of the as-prepared material (Fig.1) proves face-centred cubic NiCo₂O₄ crystalline structure (ICSD № 2421). The Reitveld refinement of the XRD data defines the lattice parameter value a = b = c = 8.110 Å. NiCo₂O₄ and Co₃O₄ have analogous patterns and cell parameters. The obtained value is much closer to that of the standard NiCo₂O₄ cell (8.114 Å) than the value for Co₃O₄ cell (0.8065 nm), ICSD № 27498.
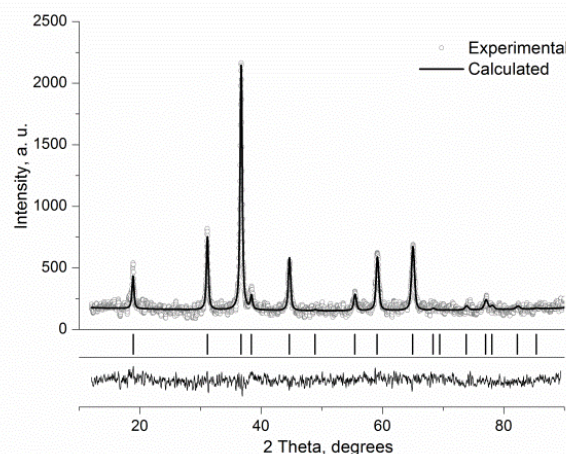

Fig. 1. X-Ray diffraction pattern of NiCo₂O₄ (open circles and Reitveld refinement (straight line). Difference between theoretical and experimental data is shown as bottom line.

Figure 2 presents the XRD patterns of NiCo₂O₄/Ag sample (a) and that of synthesized Ag (b). The peaks on the silver diffractogram define standard FCC structure of Ag (ICSD №. 053761) and lack of silver oxide peaks. In the XRD pattern of NiCo₂O₄/Ag both peaks of NiCo₂O₄ and peaks of metallic silver are visible. The NiCo₂O₄ possesses a face-centered cubic (fcc) spinel structure with $Fd\overline{3}m$ symmetry with strong (100)

orientation, where all the nickel cations are located in the octahedral positions and the cobalt cations occupy the tetrahedral and octahedral sites.
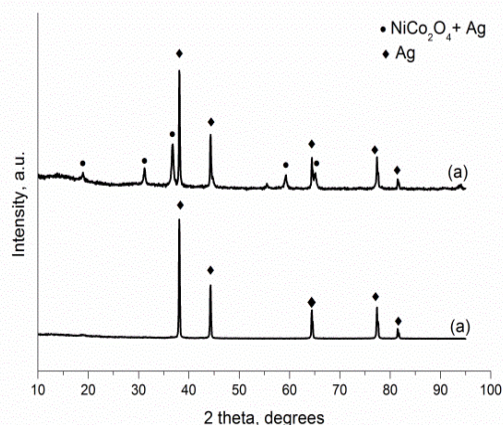

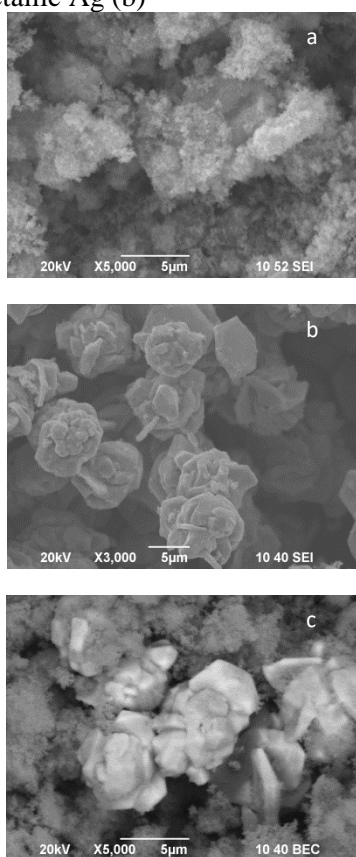**Fig. 2**. X-Ray diffraction patterns of NiCo$_2$O$_4$/Ag (a) and metallic Ag (b)

Fig. 3. SEM images: (a)NiCo$_2$O$_4$, (b)Ag, (c)NiCo$_2$O$_4$/Ag

The SEM images of pure NiCo$_2$O$_4$ (a), silver (b) and NiCo$_2$O$_4$/Ag (c) are shown in Fig. 3. The morphology of NiCo$_2$O$_4$ oxide (a) consists of nanosized spherical particles. Silver particles are bigger in size and clear visible on SEM picture of NiCo$_2$O$_4$/Ag sample (c).

The CV-curves of the studid materials depicted in Fig. 4 are conducted at room temperature with a

scan rate of 50 mVs^{-1}. The NiCo$_2$O$_4$/Ag electrode (curve II) possesses much broader area indicating a much higher capacitance as compared to the pure NiCo$_2$O$_4$ electrode (curve I). The dominant features on the forward scan are generally attributed to a change in oxidation state of Ni ions in the lattices (peaks 1 and 2). The reaction we believe is associated with:

$$Ni\,(OOH)^- \leftrightarrow Ni(OH)_2$$
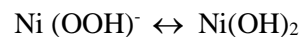
The biggest peak in the curve II, NiCo$_2$O$_4$/Ag electrode, at 0.5 mV is due to silver oxidation on the forward scan and to the silver reduction in the reverse scan (peaks 3 and 6). As concerns the peak 4 we suppose it is results of adsorption of OH- while peak 5 is due to oxygen desorption from the electrode surface. The peak 7 and 8 are due to the change in the oxidation state of silver.
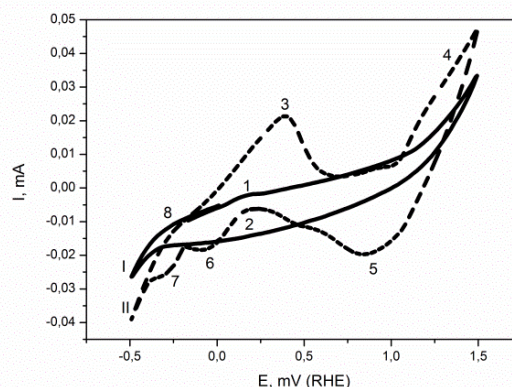

Fig. 4. Cyclic voltammograms of NiCo$_2$O$_4$ (I) and NiCo$_2$O$_4$/Ag (II) in 6M KOH

The volt-ampere (VA) curves show the catalytic activity of the NiCo$_2$O$_4$/Ag and NiCo$_2$O$_4$ electrode (fig.5) in the current density range 1–120 mA cm^{-2}. The silver addition to NiCo$_2$O$_4$ increases the catalytic activity of the electrode in ORR reaching a maximum load at current density of 20 mA cm^{-2}. The deviation in the shape of the curve observed in this graph probably is due to the oxidation of Ag to Ag$_2$O [16].
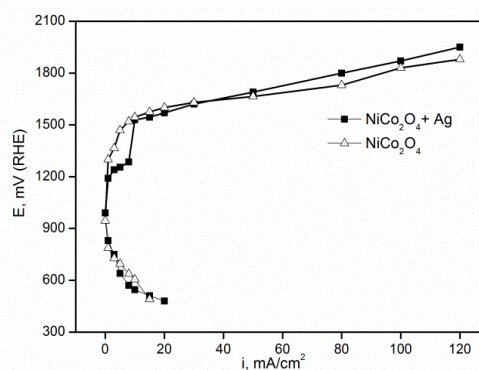

Fig. 5. Polarization curves of NiCo$_2$O$_4$ and NiCo$_2$O$_4$ /Ag

Tafel slopes for cathode and anode reaction are defined from the polarization curves (Fig.6).The Tafel slope, b, is a multifaceted parameter which can give various insights into the efficiency of a reaction. The Tafel slope at lower over potentials is 73 mV dec^{-1} for the anode reaction and 68mV dec^{-1} for the cathode reaction. The relatively low Tafel slope of the NiCo₂O₄/Ag catalyst indicates high reaction rate for low over potential input. It is often a difficult parameter to interpret as it can depend on several factors including the reaction pathway, the adsorption conditions and the active catalyst layer. The metal oxide/solution interface region consists of an inner anhydrous oxide and an outer, catalytically active hydrated region forming a surfaquo group responsible for the electrochemical activity of the oxide. Lyons and co-workers review the ORR and OER catalytic properties of transition metal oxide materials to determine the reaction mechanism [17]. They emphasize the surfaquo group concept to connect molecular catalysis and heterogeneous catalysis at hydrated oxide surfaces. The metal oxide surface possesses hydrophilic behaviours when immersed in aqueous alkaline solution. As the oxide interacts with water, solvent molecules can bond the metal cations, resulting in the transfer of a proton to a neighbouring oxygen site. Additionally not dissociated water molecules may also exist in the solution. Hence, the surface oxy groups are hydrated or hydroxylated. These hydrated surface species, named "surfaquo group", may undergo rapid redox transformations involving the simultaneous loss or gain of electrons, protons and hydroxide ions. The electrocatalytic activity of the nickel cobaltite oxide film can be ascribed to the presence of complex anionic surface groups, consisting of octahedrally co-ordinated metal complexes – the surfaquo group [17, 18]. Obviously, the electrochemical performance of NiCo₂O₄ is defined by the presence of the nickel atom with grain size similar to that of the cobalt atom. The presence of both atoms causes change in the crystal structure, in which the defects have some unexpected effects on electrochemical

performance. During the charge-discharge process, fast and reversible faradaic reactions occur on the surface of the electrode leading to the valence state changes of Co^{3+}/Co^{4+} and M^{2+}/M^{3+}(M=Co or Ni).
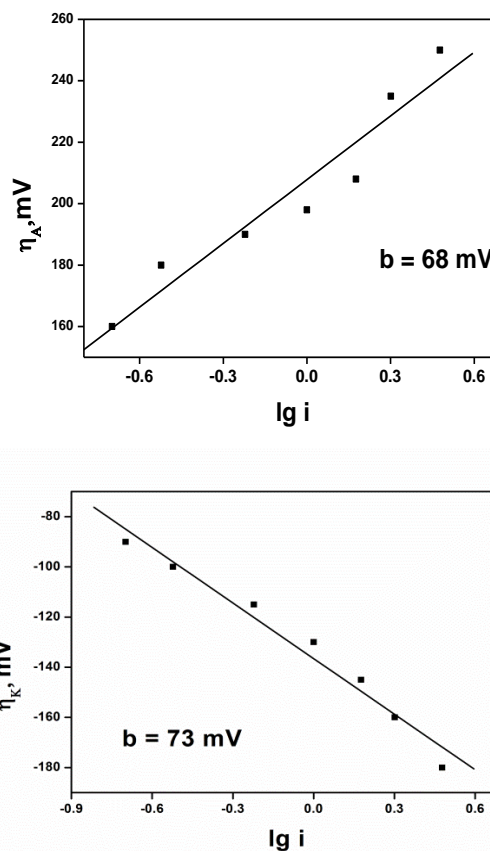

Fig. 6. Tafel plots of NiCo₂O₄/Ag: (a) anode reaction and (b) cathode reaction

The NiCo₂O₄/Ag catalyst examined as bi-functional oxygen electrode achieved 250 charge-discharge cycles without any visible structure changes (Fig.7). During the next cycles it was found to steadily degrade up to 415 charge/discharge cycles. The observed high stability of the BOE is due to both stability of the prepared NiCo₂O₄ catalyst and the design of gas diffusion electrode.
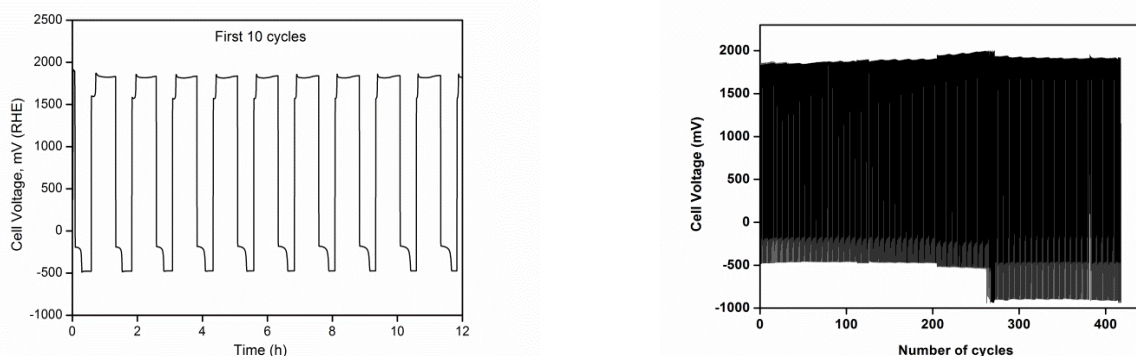

Fig. 7. Charge/discharge tests: (a) first 10 charge/discharge cycles and (b) 415 charge-discharge cycles.

71

CONCLUSIONS

$NiCo_2O_4$ catalyst synthesized through precipitation reaction possesses cubic spinel structure confirmed by XRD study. The electrode of $NiCo_2O_4$/Ag shows good catalytic activity in both oxygen reduction and evolution reactions and exhibits stable-voltage characteristics over 400 charge-discharge cycles.

REFERENCES

1. Y. Li, H. Dai, *Chem. Soc. Rev.* **43**, 5257 (2014).
2. T. Danner, S. Eswara, V. P. Schulz, A. Latz, *J. Power Sources,* **324**, 646 (2016).
3. F. Zhan, L.J. Jiang, B.R. Wu, Z.H. Xia, X.Y. Wei, G.R. Qin, *J Alloys Compd*., **293**, 804 (1999).
4. A.R. Mainar, L.C. Colmenares, J.A. Blázquez, I. Urdampilleta, *Int. J Energy Res*., 1 (2017).
5. H. Ma, B. Wang, Y. Fan, W. Hong, *Energies,* **7**, 6549 (2014).
6. M. Xu, D. Ivey, Z. Xie, W. Qu, *J. Power Sources,* **283**, 358(2015).
7. P. Sapkota, H. Kim, J. *Ind. Eng. Chem.,* **15**, 445 (2009).
8. G. Du, X. Liu, Y. Zong, T. S. A. Hor, A. Yu, Z. Liu, *Nanoscale,* **5**, 4657 (2013).
9. Y. Li, M. Gong, Y. Liang, J. Feng, J. E. Kim, H. Wang, G. Hong, B. Zhang, H. Dai, *Nat. Commun.,* **4**, 1805 (2013).
10. Z. Chen, A. Yu, R. Ahmed, H. Wang, H. Li, Z. Chen, *Electrochim. Acta,* **69**, 295 (2012).
11. P. Pei, K. Wang, Z. Ma, *Appl. Energy*, **128**, 315 (2014).
12. US Patent No. 4031 033 (1972).
13. I. Iliev, S. Gamburzev, A. Kaisheva, E. Budevski, *Bulg. Chem. Commun.*, **8**, 359 (1975).
14. M. Carey Lea, *Amer. J. Sci.,* **37**, 476 (1889).
15. B. Abrashev, D. Uzun, H. Hristov, D. Nicheva and K. Petrov, Advances in Natural Science: Theory and Application, **2**, 65 (2015).
16. H. M. A. Amin, H. Baltruschat, D. Wittmaier, K. A. Friedrich, *Electrochim. Acta,* **151**, 332 (2015).
17. R. L. Doyle, M. E.G. Lyons, Photoelectrochemical Solar Fuel Prodution, From Basic principels to Advanced Devices **2**, 92 (2016).
18. B. Marson, N. Fradette, G. Beaudoin, *J. Electrochem Soc.,* **139**, 1889 (1992).